Hindawi
Advances in Civil Engineering
Volume 2019, Article ID 9801637, 21 pages
https://doi.org/10.1155/2019/9801637

Research Article

Study of the Stability Control of the Rock Surrounding Double-Key Strata Recovery Roadways in Shallow Seams

Cheng Zhu, Yong Yuan, Zhongshun Chen, Zhiheng Liu, and Chaofeng Yuan

School of Mines, Key Laboratory of Deep Coal Resource, Ministry of Education of China, The State Key Laboratory of Coal Resources and Safe Mining, China University of Mining & Technology, Xuzhou, Jiangsu 221116, China

Correspondence should be addressed to Yong Yuan; yy20062006@163.com and Zhongshun Chen; chenzhongshun2016@163.com

Received 9 March 2019; Accepted 18 June 2019; Published 20 August 2019

Academic Editor: Xuemei Liu

The stability control of the rock surrounding recovery roadways guarantees the safety of the extraction of equipment. Roof falling and support crushing are prone to occur in double-key strata (DKS) faces in shallow seams during the extraction of equipment. Therefore, this paper focuses on the stability control of the rock surrounding DKS recovery roadways by combining field observations, theoretical analysis, and numerical simulations. First, pressure relief technology, which can effectively release the accumulated rock pressure in the roof, is introduced according to the periodic weighting characteristics of DKS roofs. A reasonable application scope and the applicable conditions for pressure relief technology are given. Considering the influence of the eroded area on the roof structure, two roof mechanics models of DKS are established. The calculation results show that the yield load of the support in the eroded area is low. A scheme for strengthening the support with individual hydraulic props is proposed, and then, the support design of the recovery roadway is improved based on the time effects of fracture development. The width of the recovery roadway and supporting parameters is redesigned according to engineering experience. Finally, constitutive models of the support and compacted rock mass in the gob are developed with FLAC3D software to simulate the failure characteristics of the surrounding rock during pressure relief and equipment extraction. The surrounding rock control effects of two support designs and three extraction schemes are comprehensively evaluated. The results show that the surrounding rock control effect of Scheme 1, which combines improved support design and the bidirectional extraction of equipment, is the best. Engineering application results show that Scheme 1 realizes the safe extraction of equipment. The research results can provide a reference and experience for use in the stability control of rock surrounding recovery roadways in shallow seams.

1. Introduction

The Shenfu and Dongsheng coalfields are the largest distribution areas of shallow seams in China. The occurrences of coal seams in this area present obvious features of shallow mining depths, thin bedrock, and thick unconsolidated strata [1, 2]. Many production practices show that the rock pressure in shallow coal seam faces is extremely high and roof falling and support crushing accidents are likely to occur [3–6]. The dynamic rock pressure is more obvious when mining under the short-distance gob of shallow seams [3, 7, 8]. In recent years, the mines in the Shenfu coalfield have generally been in a state of high-strength mining due to the excellent geological conditions and the renewal of mining equipment. The mining speed and replacement frequency of the working face have been significantly accelerated. Acceleration of the mining speed will reduce the development time of bedrock roof fractures, resulting in a significant increase in the first weighting interval and the periodic weighting interval. The migration law of the roof is more complex for double-key strata (DKS) faces, and intermittent periodic weighting typically occurs [9]. The stability control of the rock surrounding recovery roadways is key to realizing rapid equipment extraction. If the layout and support method of the recovery roadway are unreasonable, roof falling and support crushing accidents are likely to occur, as shown in Figure 1.

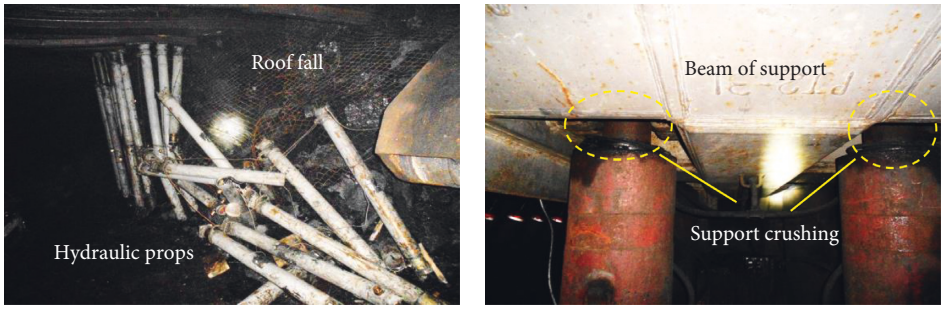

(a) (b)

Figure 1: Roof falling and support crushing accidents occurring in the recovery roadway.

This paper took the 1209 working face of the Fengjiata coal mine as the research object. The reasonable application of pressure relief technology was discussed based on the law of periodic weighting on the roof of the DKS. Considering the influence of the eroded area on the roof structure, four roof mechanics models of the DKS were established. The reasonable working resistances of the support during pressure relief and equipment extraction were calculated, improving the support design of recovery roadways and extraction schemes. Based on the above research results, the numerical simulation method was used to verify the surrounding rock control effect of the improved support design for the recovery roadway and extraction scheme.

2. Geological Setting

The Fengjiata coal mine, which is located in the east of Fugu County, is a low-gas mine. The geographical location of the mine is shown in Figure 2. The #2 coal seam is the main mining coal seam in this mine. The occurrence characteristics and mechanical properties of the coal stratum are shown in Figure 3 and Table 1. The DKS structure is present in the roof of the #2 coal seam according to the identification method of the key stratum position [10, 11].

The 1209 working face is located in the #2 coal seam. The trend length and strike length of the working face are 240 m and 1,992.5 m, respectively. The design cutting height is 3 m, and the regular circulation footage is 0.8 m. The gob roof is treated by a caving method. As shown in Figure 2, there is an eroded area in the coal to be mined. The coal seam in the eroded area is seriously eroded, and the thinnest part of the coal seam is only 1.4 m. Picks can be easily damaged when cut directly because the hardness of the eroded sandstone is relatively high. Considering various factors, such as the fault and gangue rate, rearrangement of the open-off cut was implemented. The location of the terminal line shown in Figure 2 is used to maximize the exploitation of coal resources. In the eroded area on the right side of the terminal line, the coal body is eroded to a lesser degree.

3. Pressure Relief Technology

Only a caving zone and a fracture zone exist above the longwall gob of shallow seams [10, 12–15]. Fractures develop directly toward the ground surface and cause movement and deformation [5, 16–18]. Figure 4 shows the characteristics of periodic weighting in the 1209 working face, illustrating that there is an obvious intermittent periodic weighting phenomenon. The average value of the weak periodic weighting interval is 16.7 m, and the average value of the strong periodic weighting interval is 39.7 m. For the roof of the DKS structure, the working face will appear as weak periodic weighting when the subkey stratum (SKS) is broken and the primary key stratum (PKS) is stable. At that time, the strength of the periodic weighting is relatively low because the PKS obstruct the transmission of the overburden load. When the PKS is broken, the instability load acts on the SKS, which causes the DKS to break simultaneously. Strong periodic weighting will occur on the working face at this time. The strength of strong periodic weighting is significantly higher than that of weak periodic weighting [19].

A reasonable space-time relationship between the breaking position of the DKS and the recovery roadway is critical for realizing the low-stress extraction of equipment. Pressure relief technology is based on the time effects of fracture development by controlling the advancing speed of the working face to promote the occurrence of strong periodic weighting. Thus, the rock pressure accumulated in the roof before the layout of the recovery roadway is released effectively.

3.1. Application Conditions of Pressure Relief Technology. The application location of pressure relief technology is determined based on the location of the terminal line. As shown in Figure 5, the reasonable location of pressure relief (RLPR) is as follows:

$$D = d_1 + d_2 + d_3 \leq kL_1, \tag{1}$$

where D is the distance between the RLPR and the terminal line; d_1 is the width of the weighting area, which is generally 3 times the regular circulation footage according to engineering experience; d_2 is the reserve safe distance, which is generally the regular circulation footage; d_3 is the sum of the width of the recovery roadway and the support; L_1 is the weak periodic weighting interval; and k is the safety factor that ranges from 0.4 to 0.6. In this paper, the default value of k is 0.6.

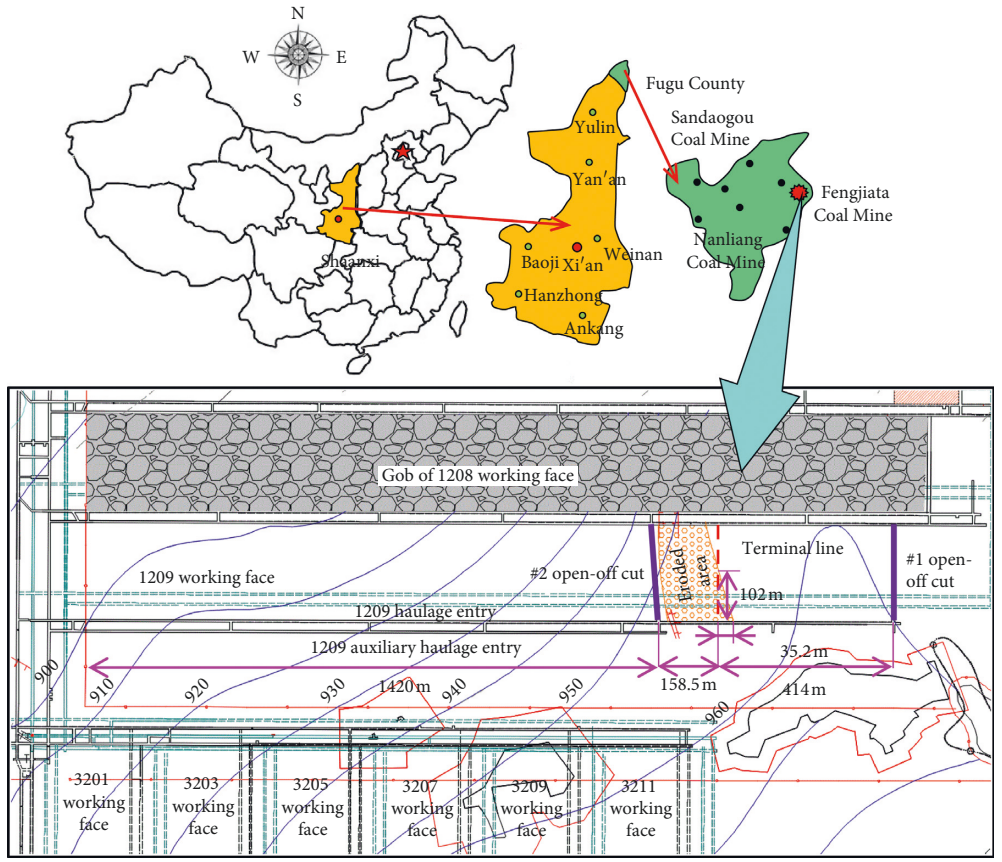

Figure 2: Geographical location of the mine and layout of the 1209 working face.

Serial number	Thickness /m	Burial depth /m	Cutline	Lithology	Position of key stratum
1	70.0	70.0		Unconsolidated stratum	
2	15.0	85.0		Coarse sandstone	Primary key stratum
3	5.30	90.3		Mudstone	
4	2.00	92.3		Pelitic siltstone	
5	3.70	96.0		Peat mudstone	
6	11.9	107.9		Medium coarse sandstone	Subkey stratum
7	2.10	110.0		Silty mudstone	
8	3.10	113.1		#2 coal seam	
9	2.60	115.7		Medium sandstone	
10	1.90	117.6		#3 coal seam	
11	5.00	122.6		Pelitic siltstone	

Figure 3: Borehole histogram of the coal stratum.

Pressure relief technology has certain applicable conditions. The technology should be applied reasonably according to the roof conditions and the law of periodic weighting.

(1) Strong periodic weighting appears in advance when the working face advances to a position closer to the RLPR. At that time, there is no need to apply pressure relief technology. The recovery roadway can

Table 1: Physical and mechanical parameters of the coal stratum.

Rock formations	Density ($kg \cdot m^{-3}$)	Friction angle (°)	Tensile strength (MPa)	Shear modulus (GPa)	Bulk modulus (GPa)	Cohesion (MPa)
Unconsolidated stratum	1760	20	0.1	0.0071	0.0125	0.019
Coarse sandstone	2586	43	11.5	14.0	18.0	3.8
Mudstone	2545	30	1.8	2.8	4.3	0.7
Pelitic siltstone	2540	35	1.0	1.6	2.7	2.0
Peat mudstone	2699	39	2.5	2.8	2.9	1.4
Medium coarse sandstone	2590	36	6.0	22.0	18.7	12.1
Silty mudstone	2500	32	1.0	1.0	2.0	2.8
#2 coal seam	1380	32	0.5	2.3	5.0	1.3
Medium sandstone	2530	29	2.0	4.7	7.5	7.5
#3 coal seam	1390	28	0.5	2.3	5.0	1.0
Pelitic siltstone	2650	38	1.8	4.9	10.8	2.8

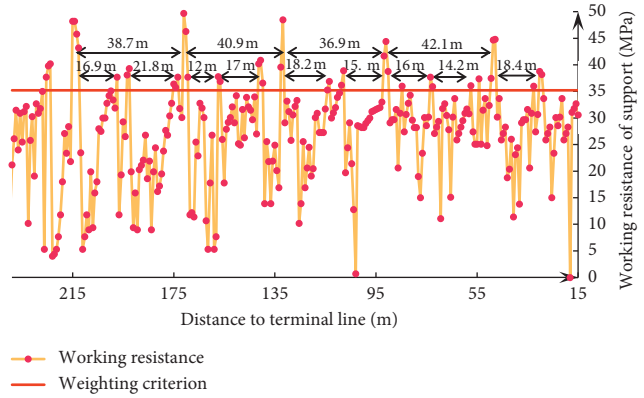

Figure 4: Working resistance curve of the support.

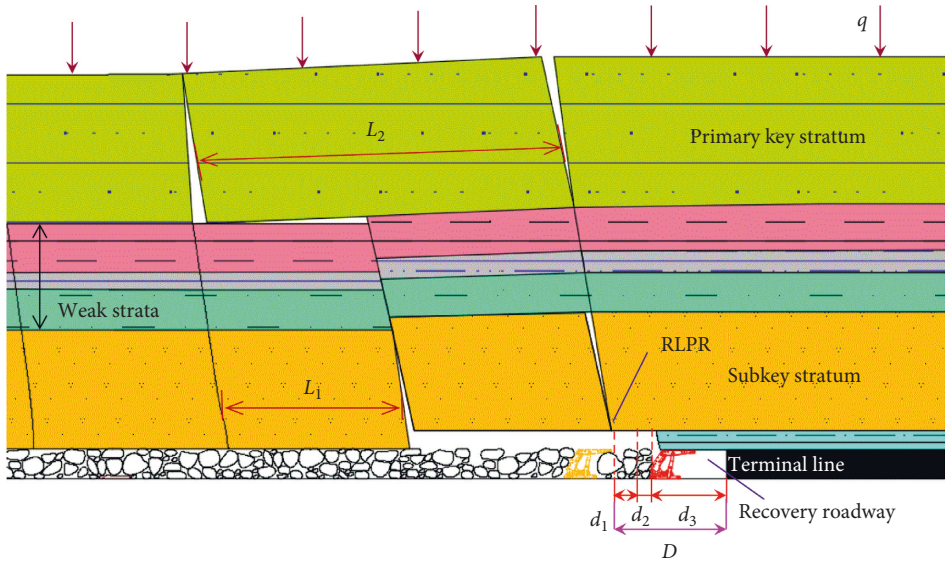

Figure 5: Location model of pressure relief.

be arranged after the working face through the weighting area.

(2) The DKS typically occur during strong periodic weighting when the working face advances to the RLPR. At that time, the working face stops advancing, and pressure relief technology should be applied. The working face continues to advance through the weighting area after indications of periodic weighting appear.

(3) The DKS remain stable when the working face advances to the RLPR. At this point, even if the working face stops advancing for a long period, no strong

periodic weighting occurs. However, the DKS are prone to strong periodic weighting when the recovery roadway is arranged. According to practical experience at the Halagou coal mine and the Xinhe coal mine, deep-hole presplitting blasting technology can be used to cut off the DKS [20, 21], thereby releasing the accumulated rock pressure in the roof.

The working face advanced to a position 13.5 m from the terminal line and 17.5 m from the previous weighting on March 18, 2018. Strong periodic weighting will soon occur in the working face, which indicates that the application conditions of pressure relief technology have been met. The reasonable working resistance of the support during the pressure relief should be studied.

3.2. Reasonable Working Resistance of the Support during Pressure Relief. The height of the caving zone can be calculated by a statistical regression formula (2).

The values of C_1 and C_2 are selected according to the type of the immediate roof, as shown in Table 2. The measured uniaxial compressive strength of silty mudstone is 33.4 MPa. The height of the caving zone of the 1209 working face is calculated as 9 m. Part of the SKS is within the range of the caving zone. The ratio of the thickness to the length of the block is more than 0.5, which indicates that a bench beam structure will be formed when the SKS is broken [9, 22, 23]:

$$\sum h = \frac{100m}{C_1 m + C_2}. \tag{2}$$

The mechanical model of the roof after pressure relief is shown in Figure 6. (I) The immediate roof caves with the advancement of the support because of its poor stability. (II) Blocks B_1 and C_1 form a bench beam structure [24] (III). The weak strata between two key strata synchronize with the SKS. (IV) Blocks B_2 and C_2 form a voussoir beam structure due to their large lengths and limited rotational space [25, 26].

In Figure 6, h_1 is the thickness of the immediate roof; h_2 is the thickness of the SKS; h_3 is the thickness of the weak strata between two key strata; h_4 is the thickness of the PKS; L_b is the length of the support beam; R_1 is the weight of the immediate roof; R_2 is the force acting on the substructure from block B_1; P_1 is the sum of the weight of block B_1 and the overlying load; P_2 is the sum of the weight of block B_2 and the overlying load; P_m is the reasonable working resistance of the support during pressure relief; θ_1 and θ_2 are the rotation angles of blocks B_1 and B_2, respectively; and W_1 and W_2 are the subsidence heights of block C_1 and C_2, respectively.

P_m can be calculated by using the following formula:

$$P_m = R_1 + R_2. \tag{3}$$

The load transfer coefficients of the bench beam structure and the voussoir beam structure are calculated by the following formulas [9, 27, 28]:

$$K_1 = \left[1 - \frac{(h_2/\sin\beta)\cos(\beta-\theta_1) + (l/2)\cos\theta_1}{(h_2/\sin\beta)\sin(\beta-\theta_1) - m + 0.3h_1}\tan\varphi_1\right], \tag{4}$$

$$K_2 = 2 + \frac{L_2\cot(\beta+\varphi_1)}{2(h_4 - m + 0.3h_1)}, \tag{5}$$

where β is the breaking angle of the key stratum and φ_1 is the friction angle between the blocks. Therefore, R_2 and P_1 can be calculated by using the following formulas, respectively:

$$R_2 = \left[1 - \frac{(h_2/\sin\beta)\cos(\beta-\theta_1) + (l/2)\cos\theta_1}{(h_2/\sin\beta)\sin(\beta-\theta_1) - m + 0.3h_1}\tan\varphi_1\right]P_1, \tag{6}$$

$$P_1 = lh_2b\gamma_2 + lh_3b\gamma_3 + \left[2 + \frac{L_2\cot(\beta+\varphi_1)}{2(h_4 - m + 0.3h_1)}\right]P_2, \tag{7}$$

where b is the width of the support; γ_2 is the bulk density of the SKS; and γ_3 is the bulk density of the weak strata.

The load P_2 is calculated by using the following formula:

$$P_2 = lh_4b\gamma_4 + 0.8\frac{L_2^2b\gamma_5}{2\tan\varphi(1-\sin\varphi)}, \tag{8}$$

where γ_4 is the bulk density of the PKS; γ_5 is the bulk density of the unconsolidated stratum; h_5 is the thickness of the unconsolidated stratum; and φ is the internal friction angle of the unconsolidated stratum.

The reasonable working resistances of the supports outside and inside the eroded area are calculated using the following formulas, respectively.

$$P_m = L_bh_1b\gamma_1 + \left[1 - \frac{(h_2/\sin\beta)\cos(\beta-\theta_1) + (l/2)\cos\theta_1}{(h_2/\sin\beta)\sin(\beta-\theta_1) - m + 0.3h_1}\tan\varphi_1\right] \left\{lh_2b\gamma_2 + lh_3b\gamma_3 + \left[2 + \frac{L_2\cot(\beta+\varphi_1)}{2(h_4 - m + 0.3h_1)}\right]\left(L_2h_4b\gamma_4 + 0.8\frac{L_2^2b\gamma_5}{2\tan\varphi(1-\sin\varphi)}\right)\right\}, \tag{9}$$

$$P_m = \left[1 - \frac{((h_1+h_2)/\sin\beta)\cos(\beta-\theta_1) + (l/2)\cos\theta_1}{((h_1+h_2)/\sin\beta)\sin(\beta-\theta_1) - m}\tan\varphi_1\right] \left\{l(h_1+h_2)b\gamma_2 + lh_3b\gamma_3 + \left[2 + \frac{L_2\cot(\beta+\varphi_1)}{2(h_4 - m + 0.3h_1)}\right]\left(L_2h_4b\gamma_4 + 0.8\frac{L_2^2b\gamma_5}{2\tan\varphi(1-\sin\varphi)}\right)\right\}. \tag{10}$$

Table 2: Values of the coefficients C_1 and C_2 for various stratum strengths.

Type of immediate roof	Uniaxial compressive strength (MPa)	Coefficient	
		C_1	C_2
Strong and hard	>40	2.1	16
Medium strong	20~40	4.7	19
Soft and weak	<20	6.2	32

Σh is the height of the caving zone, and m is the mining height.

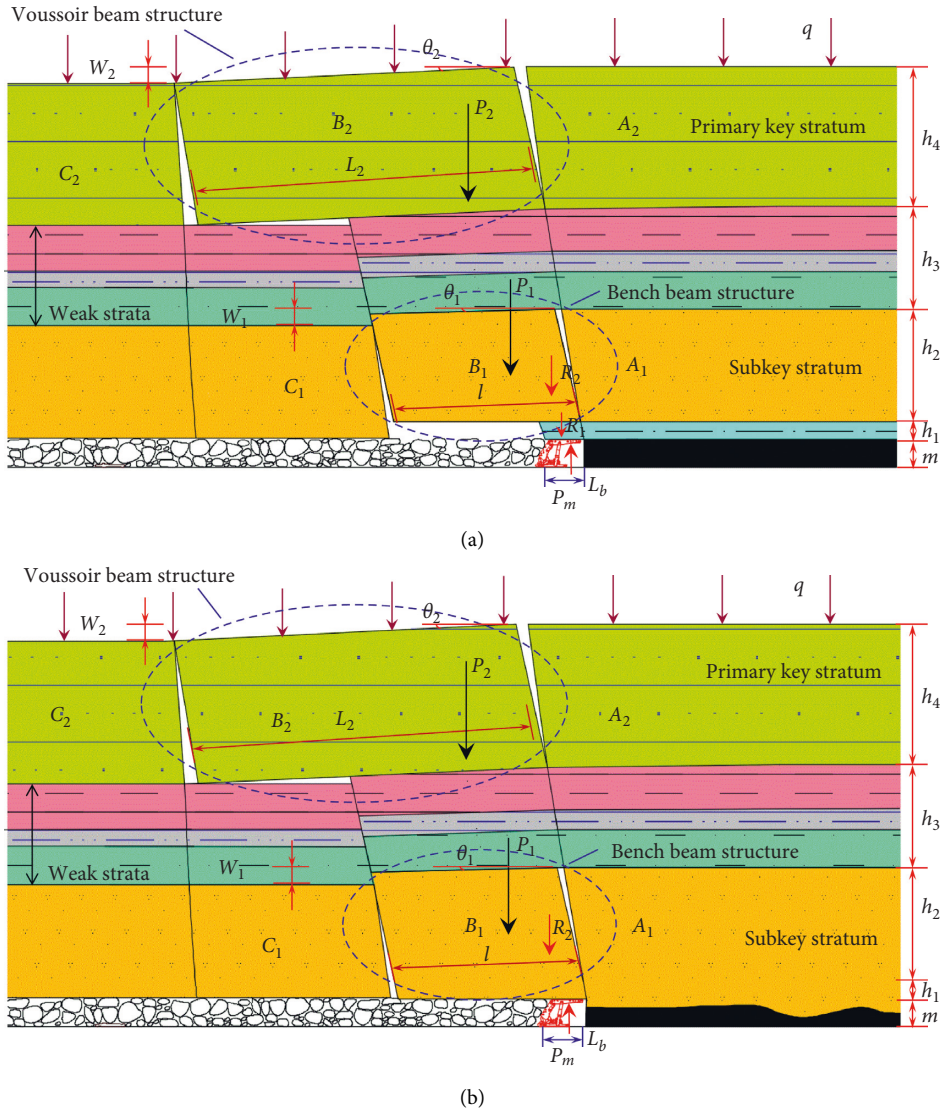

Figure 6: Mechanical model of the roof after pressure relief. (a) Outside the eroded area. (b) Inside the eroded area.

The 1209 working face was equipped with 141 ZY9500/17/35D-type supports. The length L_b and width b of the support beam are 4.5 m and 1.75 m, respectively. The lengths of block B_1 and block B_2 are 17.5 m and 36 m, respectively, after pressure relief. The rotation angle of a block in a shallow seam is generally in the range from 4° to 6°. Suppose that the value of θ_1 is 4°. Referring to the research results of Huang et al., the breaking angle β of the key stratum is 90° and the friction angle φ_1 between blocks is 44.3° [9]. From Figure 3 and Table 1, the loads P_m on the support outside and inside the eroded area are calculated to be 4,807.6 kN and 10,022.3 kN, respectively. This figure shows that the yield load of the support inside the eroded area is somewhat low. Roof falling and support crushing are prone to occur inside the eroded area during pressure relief. Therefore, individual hydraulic props are installed on both sides of the hydraulic support as reinforcement (https://www.sciencedirect.com/science/article/pii/S1350630717304120?via%3Dihub). Table 3 lists the parameters of the individual hydraulic props. The support resistance of the support was raised to approximately 10,100 kN.

Table 3: Technical parameters of individual hydraulic props.

Type	Height (m)	Setting load (kN)	Yield load (kN)
DZ35-30/110Q	2.7~3.5 m	144~188	300

4. Support Design of Recovery Roadways

The extraction technology of the longwall face is mainly divided into shearer driving roadway technology and predriven roadway technology. The traditional shearer driving roadway technology is mainly applied to mines with limited funds and geological conditions and has the disadvantage of a long extraction cycle. Predriven roadway technology also has obvious shortcomings, such as relatively large work quantities, high maintenance costs, and a high roof fall likelihood when crossing the predriven roadway. At present, this technology is mainly used in mines with simple geological conditions in the Shendong mining area. Most mines in China still apply shearer driving roadway technology. The roof of the recovery roadway is supported by the coal wall-supporting structure-hydraulic support-gob (CSHG) structure as a whole. Therefore, the design of the support parameters and the reasonable working resistance of the supports should be studied to achieve rapid and safe extraction.

4.1. Improvement of the Support Design. Resin mesh is laid on the working face after strong periodic weighting. The shearer cuts the coal wall to arrange the recovery roadway after the working face passes through the weighting area. The initial support design determined by analogous experience is shown in Figure 7.

The original plan was to unidirectionally extract the supports from the haulage entry after the initial support design was completed. However, the actual application effect of the plan for the 1208 working face was not satisfactory. The deformation of the surrounding rock of the recovery roadway was large, which affected normal extraction. Thirty-two days were required to complete all extraction tasks for the 1208 working face.

The initial support parameters and extraction technology were improved as follows:

(1) Considering the low support efficiency and time-consuming construction of the rockbolts near the gob, four wire ropes were used instead of five rows of rockbolts near the gob, saving 194 hours of work time.

(2) According to past experience, the support can be successfully extracted when the width of the recovery roadway is half the length of the support. The length of ZY9500/17/35D-type support is 6.92 m. Considering that the regular circulation footage is 0.8 m and the space of a certain width should be reserved, the width of the recovery roadway was changed from 5 m to 4.2 m.

(3) The length of the rockbolt was changed from 2.2 m to 2.5 m to enhance the roof support. The depth of the anchored bedrock was increased, and the roof stability was enhanced.

(4) The supports were bidirectionally extracted from the middle of the recovery roadway.

JDPET200 × 200MS resin mesh with a size of 260 m × 25 m was selected. The row spacing and column spacing of the flank rockbolts were 800 mm × 1,500 mm. The steel beam is made of round steel of Φ16 mm × 6,000 mm. Each steel beam connects six rockbolts (anchor cable). The wire rope is Φ16 mm × 260 m.

4.2. Reasonable Working Resistance of the Supports. D is observed to be 13.5 m in Figures 7 and 8, which cannot satisfy formula (1). The SKS easily ruptures along the coal wall, and weak periodic weighting occurs. Therefore, the mechanical model of the roof shown in Figure 9 was established to calculate the reasonable working resistance of the support.

The reasonable working resistance P_z of the supports outside and inside the eroded area during the extraction of supports is shown in the following formulas, respectively:

$$P_z = L_k h_1 b\gamma_1 + \left[1 - \frac{(h_2/\sin\beta)\cos(\beta-\theta_1) + (D/2)\cos\theta_1}{(h_2/\sin\beta)\sin(\beta-\theta_1) - m + 0.3h_1} \cdot \tan\varphi_1\right](Dh_2 b\gamma_2 + Dh_3 b\gamma_3), \tag{11}$$

$$P_z = \left[1 - \frac{((h_1+h_2)/\sin\beta)\cos(\beta-\theta_1) + (D/2)\cos\theta_1}{((h_1+h_2)/\sin\beta)\sin(\beta-\theta_1) - m} \cdot \tan\varphi_1\right] \cdot [D(h_1+h_2)b\gamma_2 + Dh_3 b\gamma_3], \tag{12}$$

where L_k is the sum of the widths of the recovery roadway and the support.

According to the improved support design, L_k is 11.1 m and D is 13.5 m. The calculated P_z values are 3970.8 kN and 4764.6 kN, respectively. Considering that the actual efficiency of the supports is 0.9, the reasonable working resistance of the support is no less than 5294 kN. The ZY9500/17/35D-type support can meet the requirements for roof control.

5. Numerical Simulation of Surrounding Rock Control

Considering the influence of the eroded area on the recovery roadway, the working face model was established using FLAC3D software, as shown in Figure 10. The X direction of the model was the advancing direction of the working face, and the Y direction was the layout direction of the working face. Modeling was completed to the ground surface in the Z direction. The blocks in the study area were finely divided with a size of 0.4 m × 0.8 m × 0.5 m. An M-C constitutive

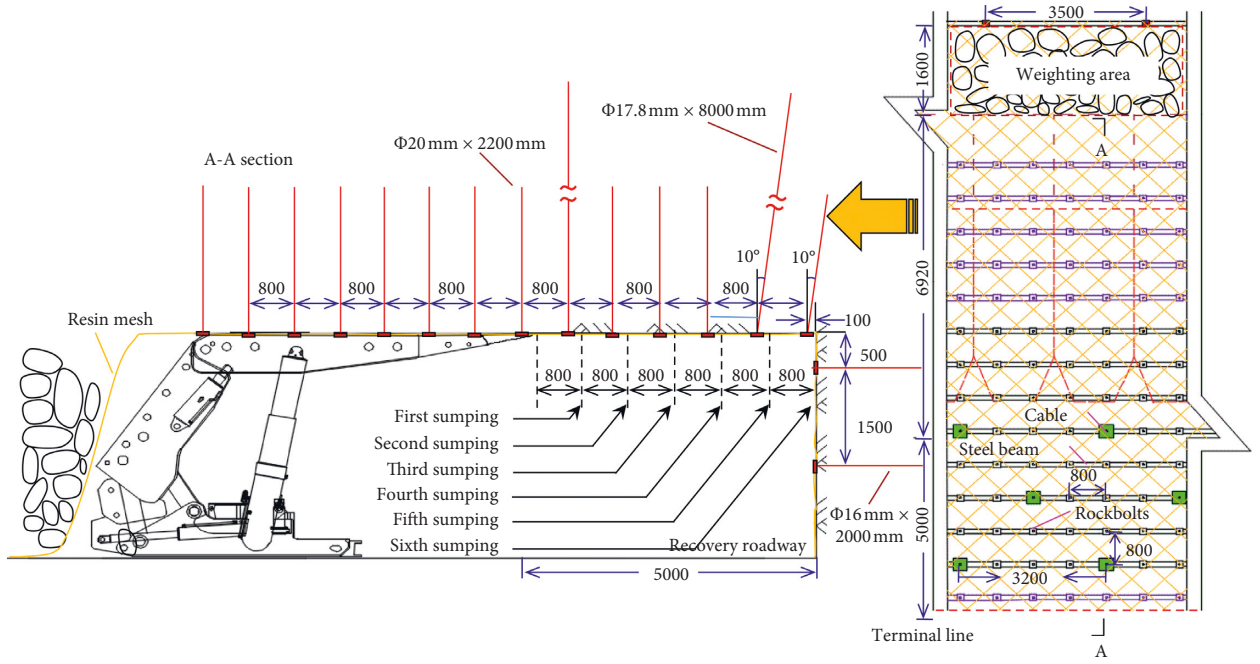

Figure 7: Initial support design of the recovery roadways.

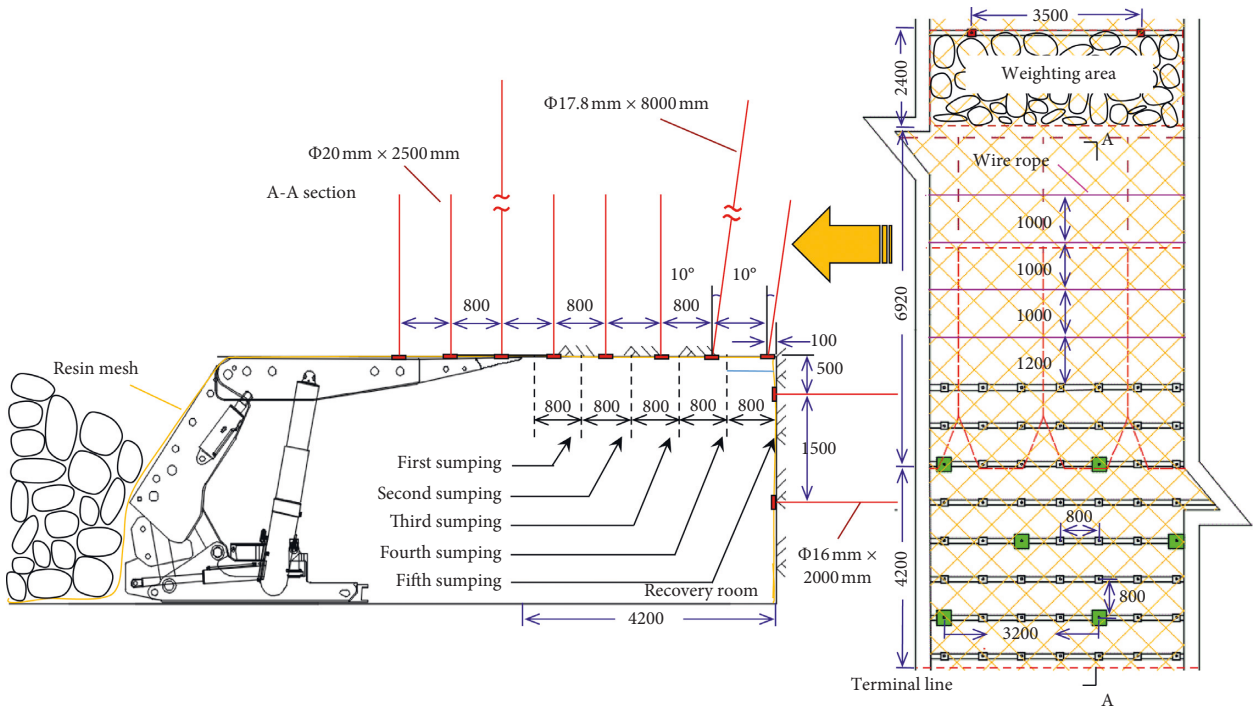

Figure 8: Improved support design of the recovery roadway.

model was employed, and five sections were laid along the working face.

Based on compaction theory, the constitutive model of the gob was established using the FISH language [29–31]. The initial mechanical parameters of the gob are shown in Table 4. The modulus and strength of the caved rock mass in the gob increased continuously under the action of the overlying load. The vertical strains of all zones in the gob were monitored because there is a functional relationship between the bulk modulus and the vertical strain. The bulk modulus of the gob was updated continuously according to the vertical strains induced during roof convergence, and the gob recovered vertical stress also changed spontaneously.

The gob-recovered vertical stress compares well with that of the Salamon model, as shown in Figure 11. The numerical simulation results are consistent with the

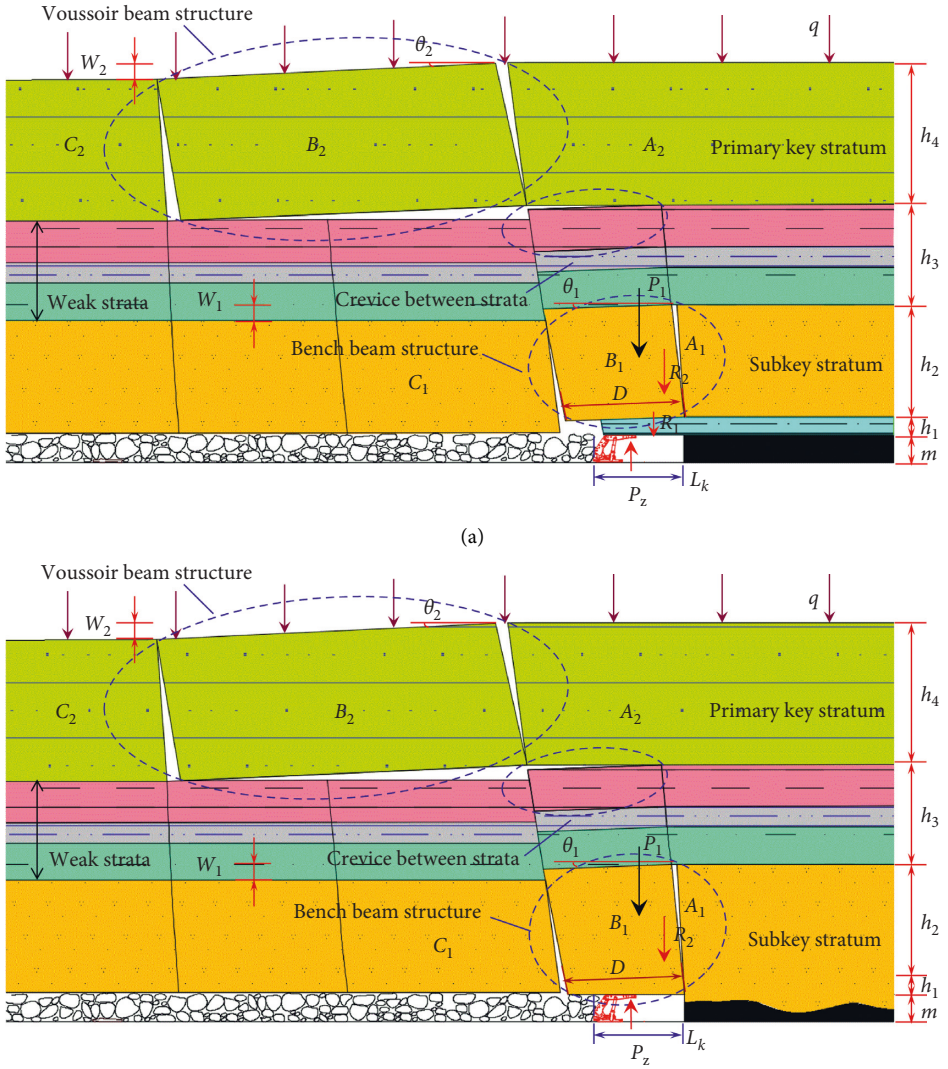

Figure 9: Mechanical model of the roof during the extraction of supports. (a) Outside the eroded area. (b) Inside the eroded area.

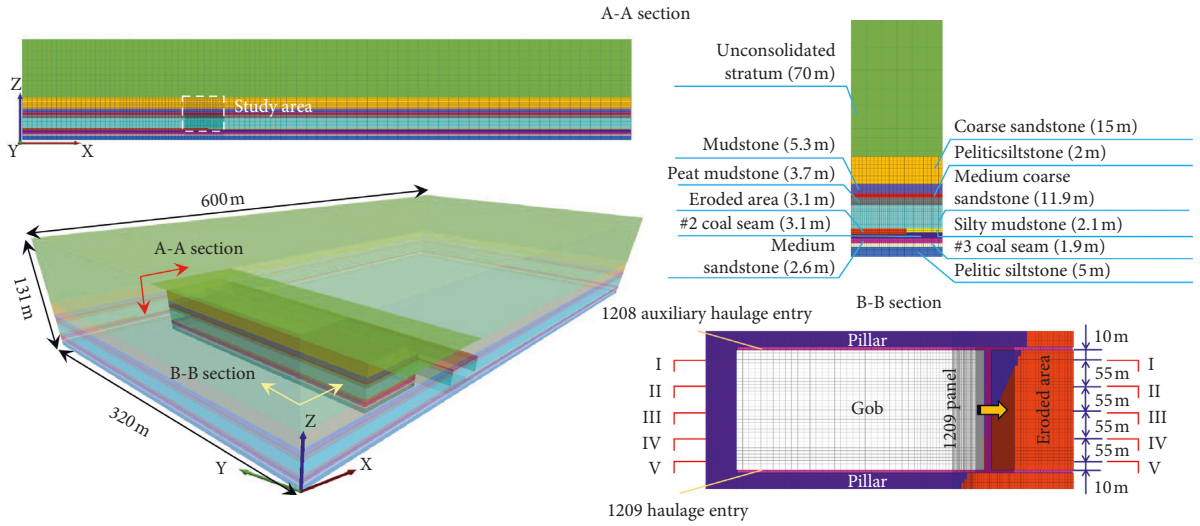

Figure 10: Numerical model of the working face.

Table 4: Numerical simulation parameters of the gob.

Bulk modulus (MPa)	Shear modulus (MPa)	Density (kg·m^{-3})	Friction angle (°)	Cohesion (MPa)	Tensile strength (MPa)
0.497	0.298	1800	5	0.001	0

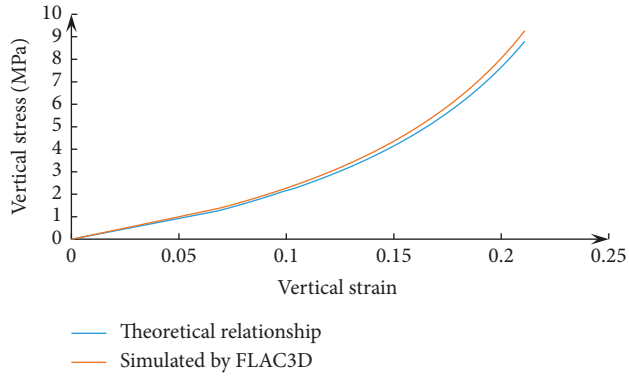

Figure 11: Relationship between the vertical stress and vertical strain.

theory, and the constitutive model of the gob is reasonable.

A constitutive model of the support was established at the same time. Figure 12 is a model of a single support, wherein the roof above the face width is supported by upwardly applied grid forces. The resultant force of the grid force is the working resistance of a support. The working characteristics of the grid force are determined based on the characteristic curve of the support. The setting load of the grid force is considered to be 60% of the yield load. The grid force enters a constant stage when the vertical displacement of the grid point reaches 0.2 m. The vertical displacement-grid force curve of a grid point is monitored, as shown in Figure 12. The working resistance of the support can be reasonably exerted.

5.1. Simulation of Pressure Relief. After the working face was advanced to the RLPR in the model, the equilibrium state was calculated to examine the pressure relief technology. The plastic zone distribution of five sections was obtained after pressure relief, as shown in Figure 13. We added the symbol of support in Figure 13 to visualize the pressure relief. There is no plastic zone in the gob because the elastic model was used to establish the constitutive model of the gob. Shear-tension failure occurs in the PKS due to the load of the unconsolidated stratum. Shear failure along the coal wall occurs in the SKS and weak strata under the superposition of the instability load of the PKS and the load of the unconsolidated stratum. The numerical simulation results show that the DKS will be broken simultaneously after pressure relief.

5.2. Simulation of the Support Design for the Recovery Roadway. The recovery roadway was arranged according to the terminal line after pressure relief. A linear element was used to simulate the linking effect of the resin mesh and steel beams. A cable element was used to simulate the anchor cables and rockbolts. The wire rope was not simulated in the model. A node-node connection was established between the structural elements to achieve a combined support effect. The mechanical parameters of the structural units are shown in Table 5. Numerical models for the two kinds of supporting design are shown in Figure 14. The excavation of the model and the installation of the supporting structure are consistent with the actual construction process.

Figures 15 and 16 show the distribution of the plastic zone and the roof subsidence curves, respectively, after the two kinds of support designs were simulated.

Several conclusions can be drawn from the results: (I) The lithology of the immediate roof is weak, and plastic failure occurs during the simulation of roadway support. At that time, the DKS remain stable. (II) More time steps were calculated in the initial support design because of the complexity of construction. Therefore, the plastic zone distribution and the roof subsidence of the initial support design are higher than those of the improved support design. (III) The difference between the roof subsidence curves is largest outside the eroded area. The roof subsidence of the recovery roadway is close to the fulcrum of the roof rotation and is small due to the tensile properties of the anchor cable. The roof subsidence above the face width increased monotonically. The roof subsidence after the face width is the largest due to the weak supporting strength and the distance from the fulcrum of the roof rotation. (IV) The plastic zone distribution and roof subsidence in the eroded area are lower than those outside the erosion zone.

5.3. Simulation of the Surrounding Rock Control Effect during the Extraction of Equipment. After the recovery roadway was arranged, the following three schemes were proposed

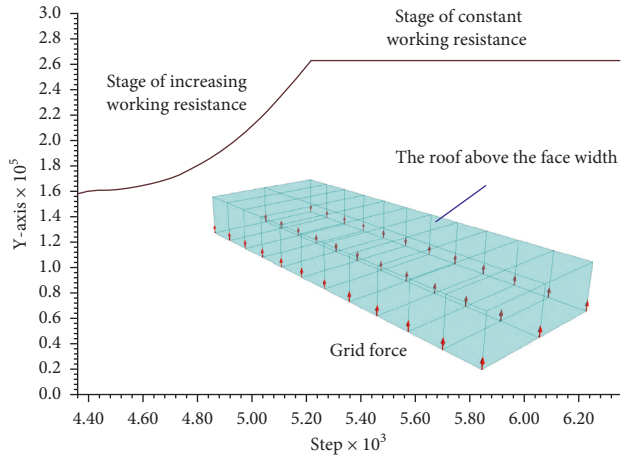

Figure 12: Numerical model of the grid force.

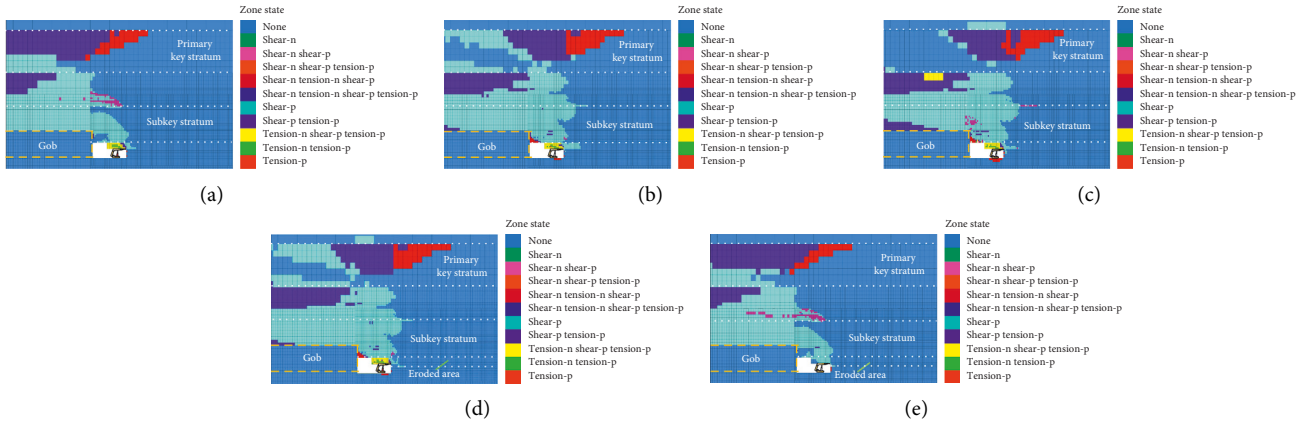

Figure 13: Plastic zone distribution of the five sections. (a) I-I. (b) II-II. (c) III-III. (d) IV-IV. (e) V-V.

Table 5: Mechanical parameters of rockbolts and cables.

	Elastic modulus (GPa)	Cross-sectional area (m^2)	Tensile strength (MPa)	Stiffness of anchorage agent (GPa)	Cohesion of anchorage agent (MN/m)
Rockbolts	20	0.000314	250	5.35	0.42
Flank rockbolt	20	0.0002	200	5.35	0.42
Cables	200	0.000248	1900	5.35	0.42
Resin mesh	0.0065	–	–	–	–

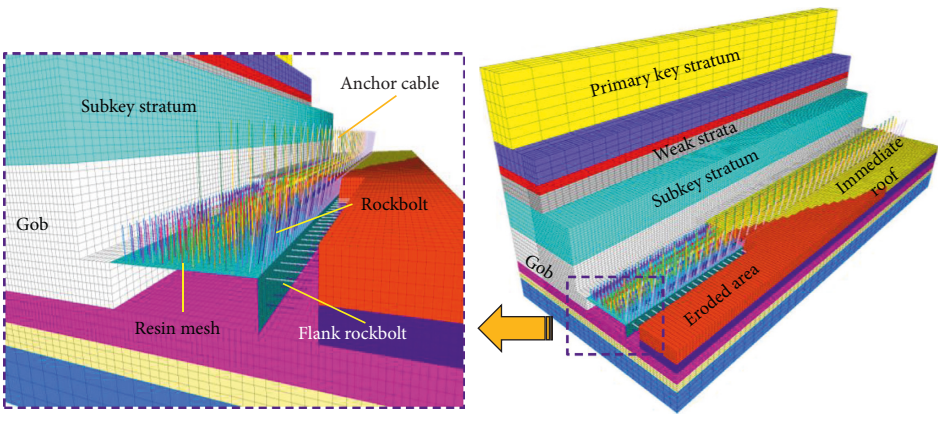

(a)

Figure 14: Continued.

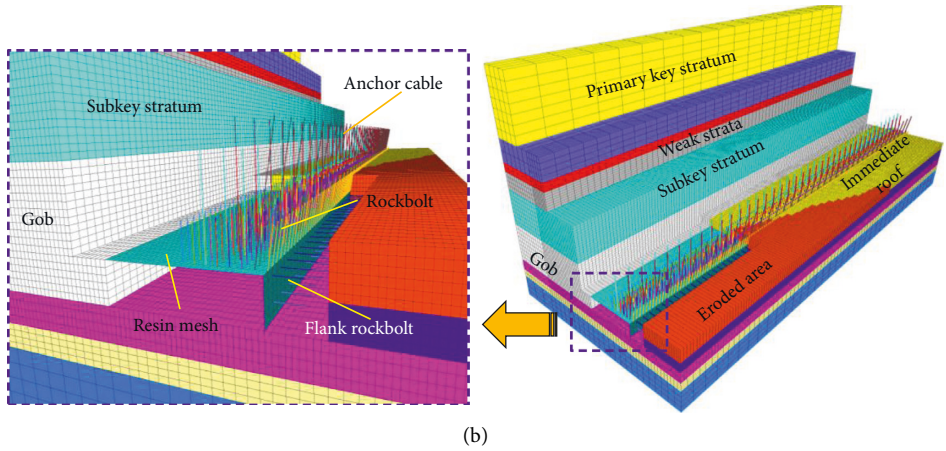

Figure 14: Numerical models for two kinds of support designs. (a) Initial support design. (b) Improved support design.

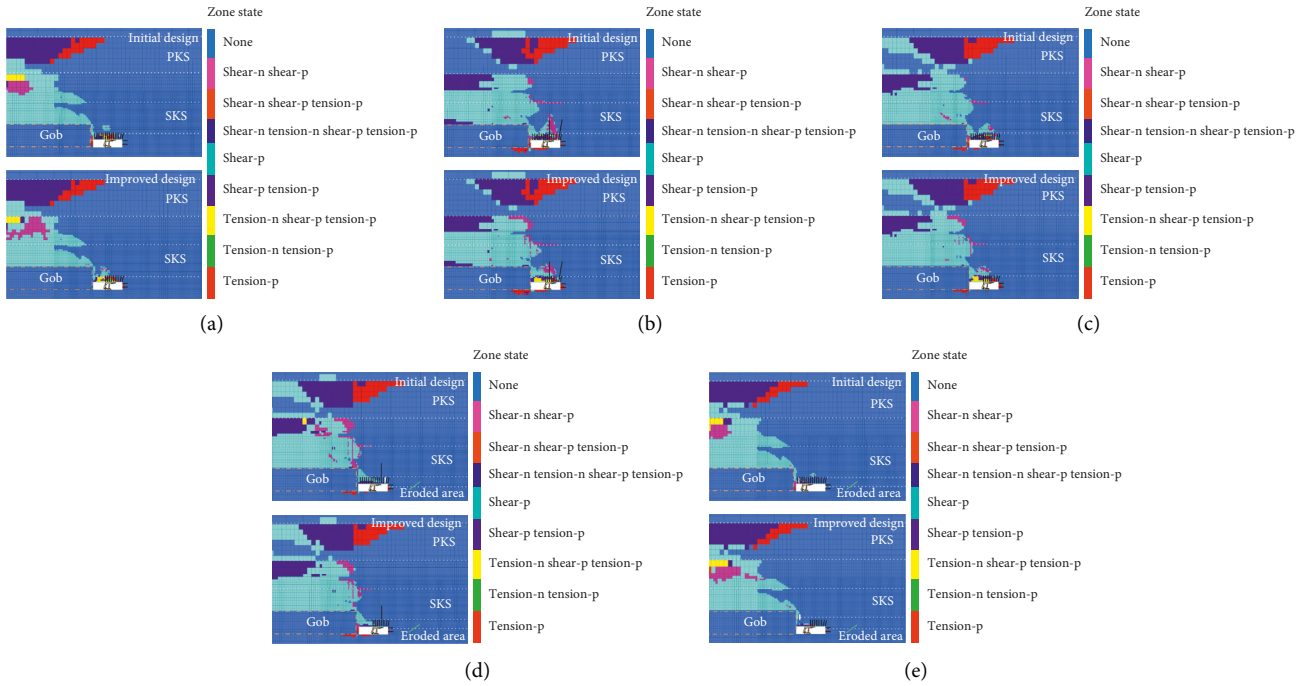

Figure 15: Plastic zone distribution of the two support parameter designs. (a) I-I. (b) II-II. (c) III-III. (d) IV-IV. (e) V-V.

in the model: (I) bidirectionally extract the supports from the middle of the roadway after applying the improved support design (Scheme 1), (II) bidirectionally extract the supports from the middle of roadway after applying the initial support design (Scheme 2), and (III) unidirectionally extract the supports from the haulage entry after applying the initial support design (Scheme 3).

As shown in Figure 17, the support extraction process is divided into three stages. The number of time steps of unidirectional extraction is twice that of bidirectional extraction when the same number of supports is extracted. The extraction of supports was simulated by canceling the grid force applied to the grid point.

To qualitatively analyze the surrounding rock control effect of the three schemes, 20 time steps were calculated in the model in accordance with the extraction of a support. In Stage I of Schemes 1 and 2, 200 time steps are calculated, and 400 time steps are calculated in Scheme 3. The plastic zone distribution and the roof subsidence curve are shown in Figures 18 and 19, respectively.

The following conclusions can be drawn: (I) The roof subsidence of each section in Scheme 1 is the smallest, followed by that in Scheme 2 and then that in Scheme 3. (II) In Schemes 1 and 2, the roof subsidence of section II-II is the largest, while in Scheme 3, the roof subsidence of section I-I is the largest. (III) Penetrating plastic damage occurs in the

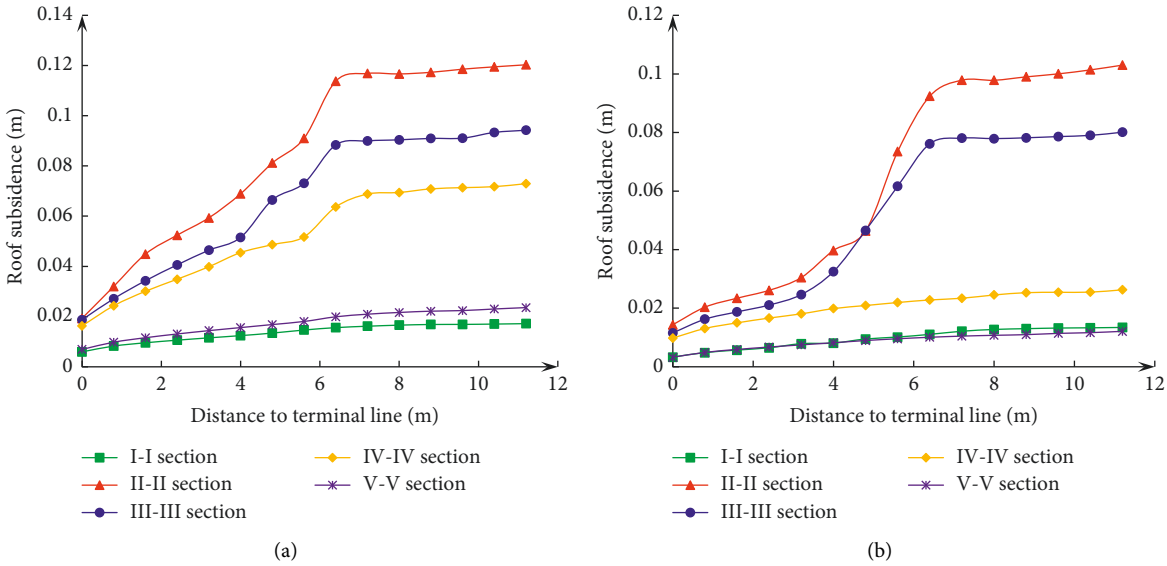

Figure 16: Roof subsidence curves of the two support designs. (a) Initial design. (b) Improved design.

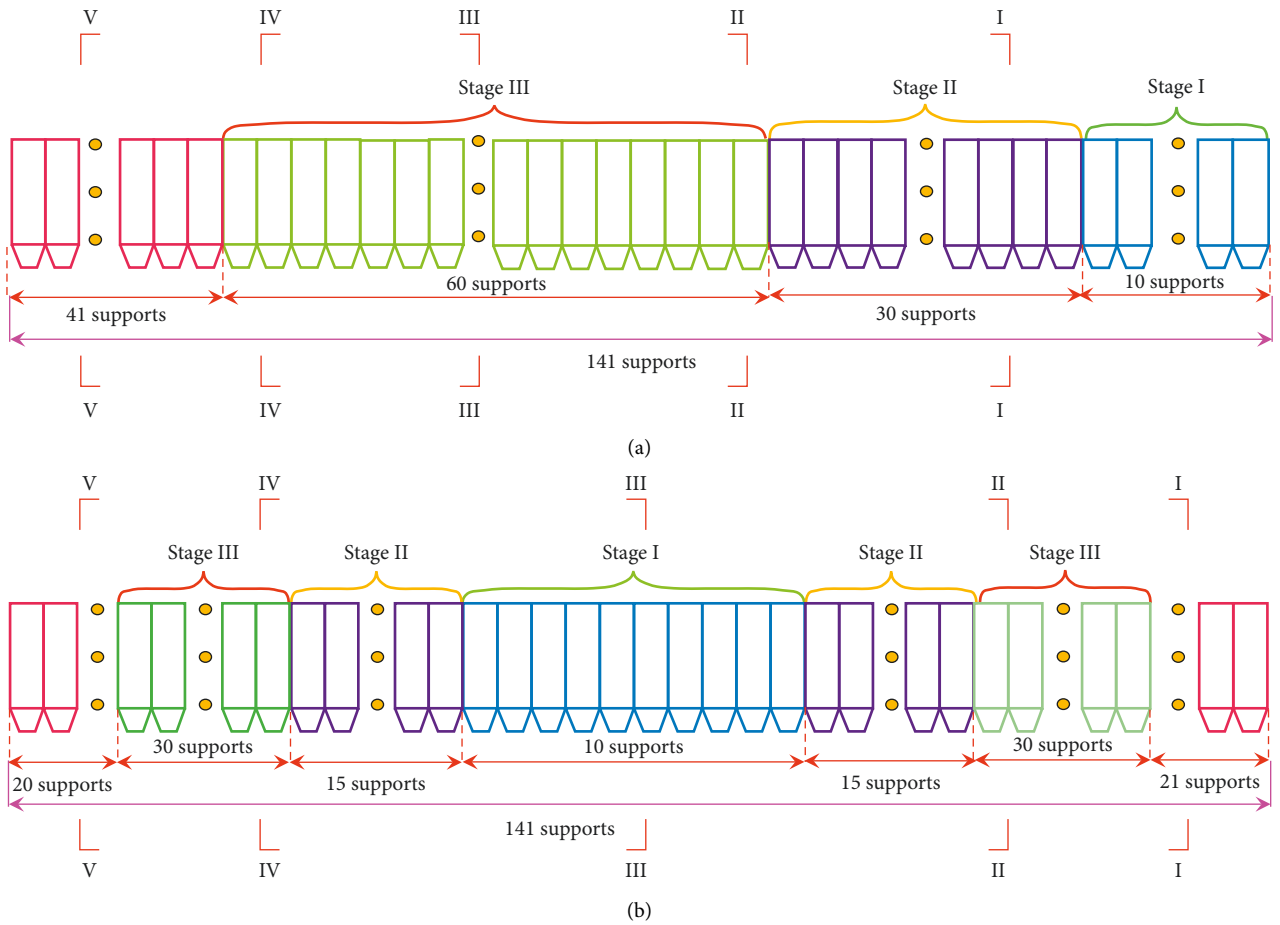

Figure 17: Schematic diagram of the two extraction processes. (a) Unidirectional extraction process. (b) Bidirectional extraction process.

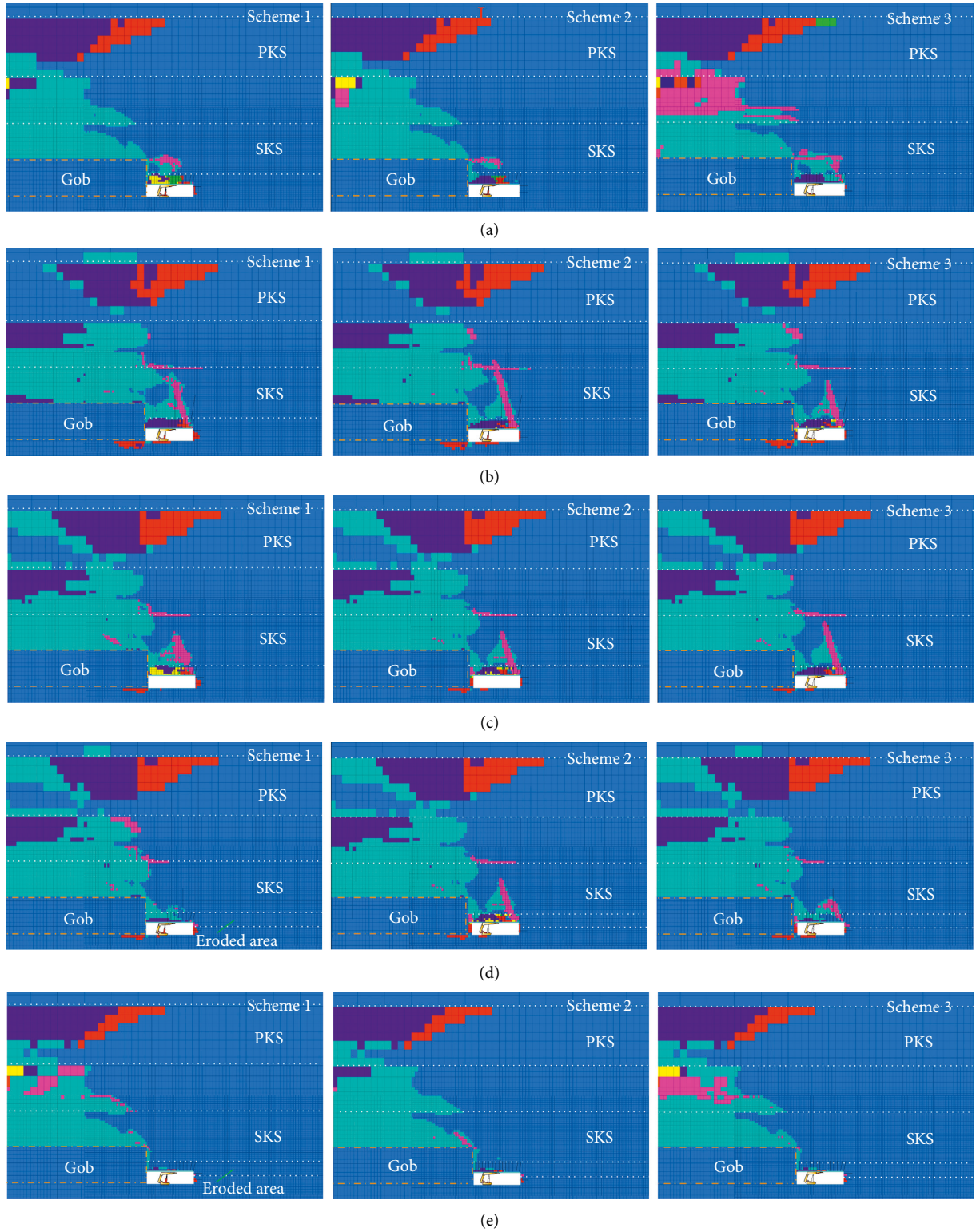

Figure 18: Plastic zone distribution of Stage I. (a) I-I. (b) II-II. (c) III-III. (d) IV-IV. (e) V-V.

SKS of section II-II. The concentrated area of rock pressure is still located in the middle of the recovery roadway. However, the stability of the surrounding rock is enhanced due to its proximity to the eroded area.

In Stage II of Schemes 1 and 2, 600 time steps are simulated, and in Scheme 3, 1,200 time steps are simulated. The plastic zone distribution and roof subsidence curve are shown in Figures 20 and 21, respectively.

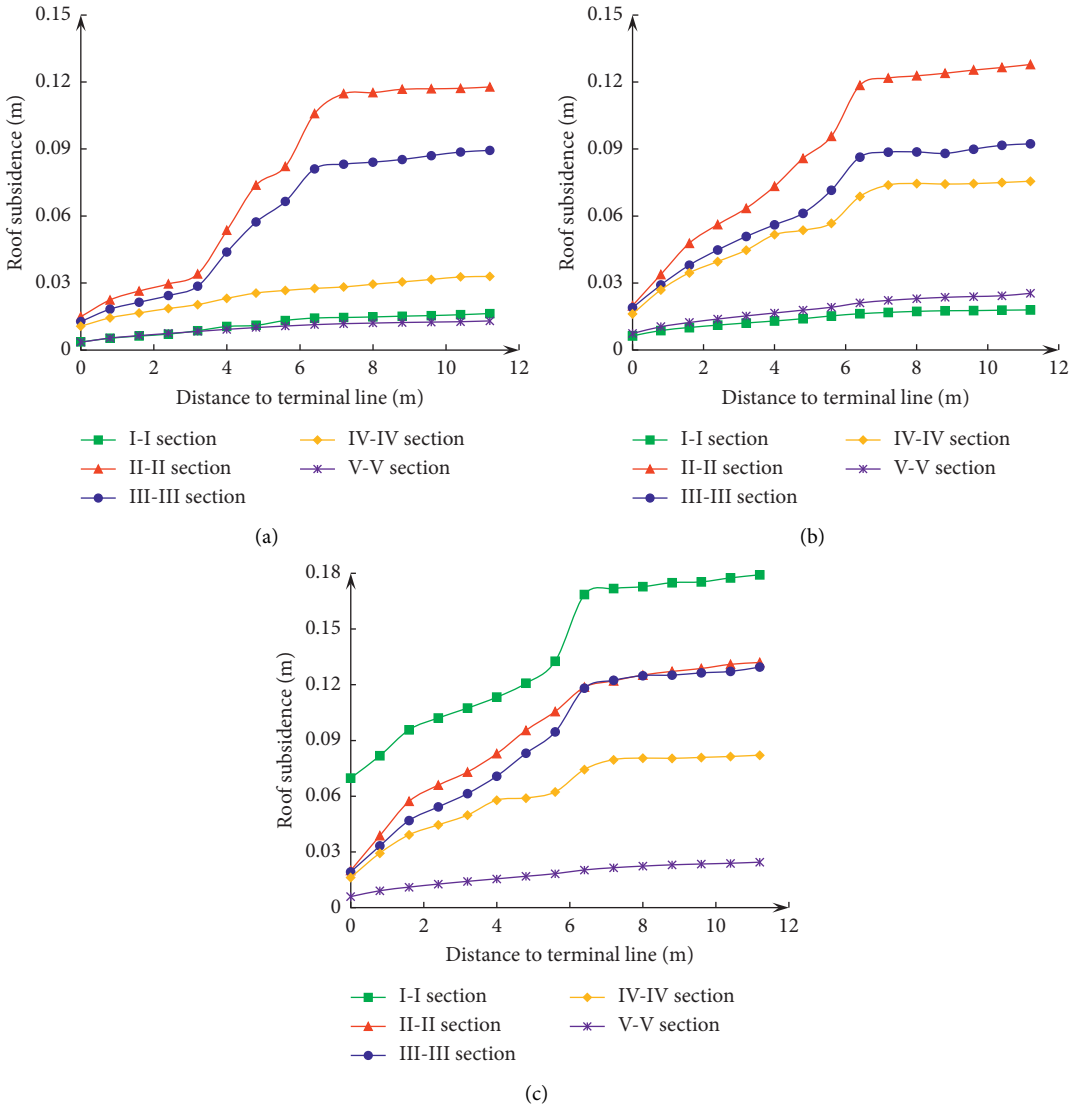

Figure 19: Roof subsidence curves of Stage I. (a) Scheme 1. (b) Scheme 2. (c) Scheme 3.

The following conclusions can be drawn: (I) The difference in the roof subsidence curves in the area where the support has been extracted is reduced. (II) The roof subsidence of section II-II near the recovery roadway increases significantly in Schemes 1 and 2. (III) The roof subsidence rate is accelerated because the supporting intensity behind the support is low in section II-II of Scheme 1. (IV) The surrounding rock control effect of Scheme 1 is the best in Stage II.

In Stage III of Schemes 1 and 2, 1,200 time steps are simulated, and in Scheme 3, 2,400 time steps are calculated. The plastic zone distribution and roof subsidence curve are shown in Figures 22 and 23, respectively.

After Stage III, most of the supports in the recovery roadway have been extracted. At this time, the following conclusions can be drawn: (I) In Schemes 2 and 3, significant plastic damage is observed in the DKS and the weak strata. However, the stability of the PKS is not significantly affected in Scheme 1. (II) The roof subsidence of Scheme 3 is still significantly higher than those of the other schemes. (III) The roof subsidence of section I-I in Scheme 1 is lower than that in Scheme 2.

After comprehensively evaluating the control effect of the surrounding rock, Scheme 1 is applied to the construction site of the recovery roadway in the 1209 working face.

6. Engineering Applications

Considering that the immediate roof will fall when the support underneath is extracted, wooden cribs are usually arranged to support the immediate roof, which ensures the smooth extraction of adjacent supports. As shown in Figure 24, the field application shows that the surrounding rock control effect of Scheme 1 is ideal, and

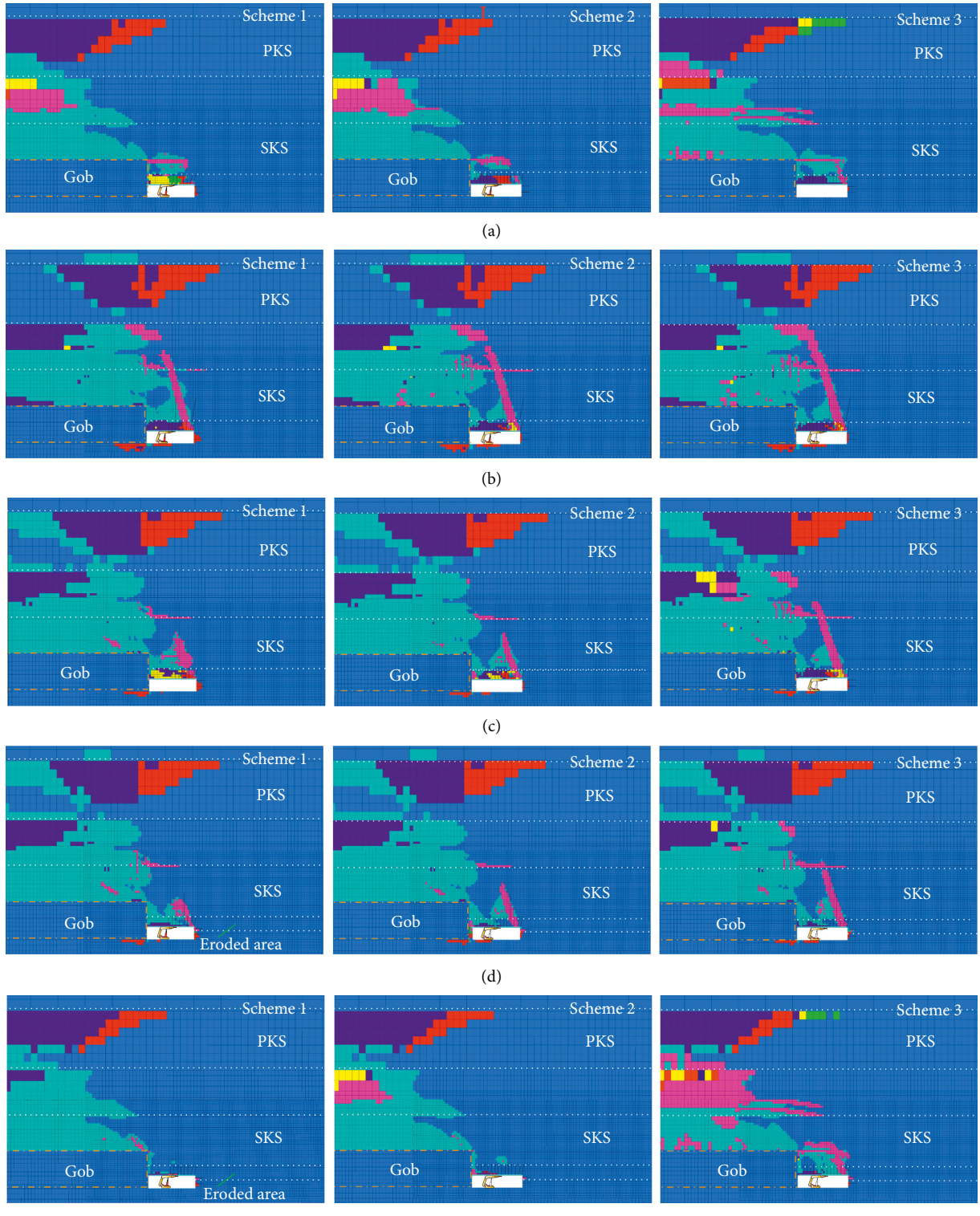

Figure 20: Plastic zone distribution of Stage II. (a) I-I. (b) II-II. (c) III-III. (d) IV-IV. (e) V-V.

there is no roof falling or support crushing. Only 14 days were required from laying the resin mesh to extracting all the supports. Compared with that of the 1208 working face, the extraction time was shortened by 18 days, representing 1.07 million RMB in savings. Thus, this method realizes the safe, economical, and rapid extraction of equipment.

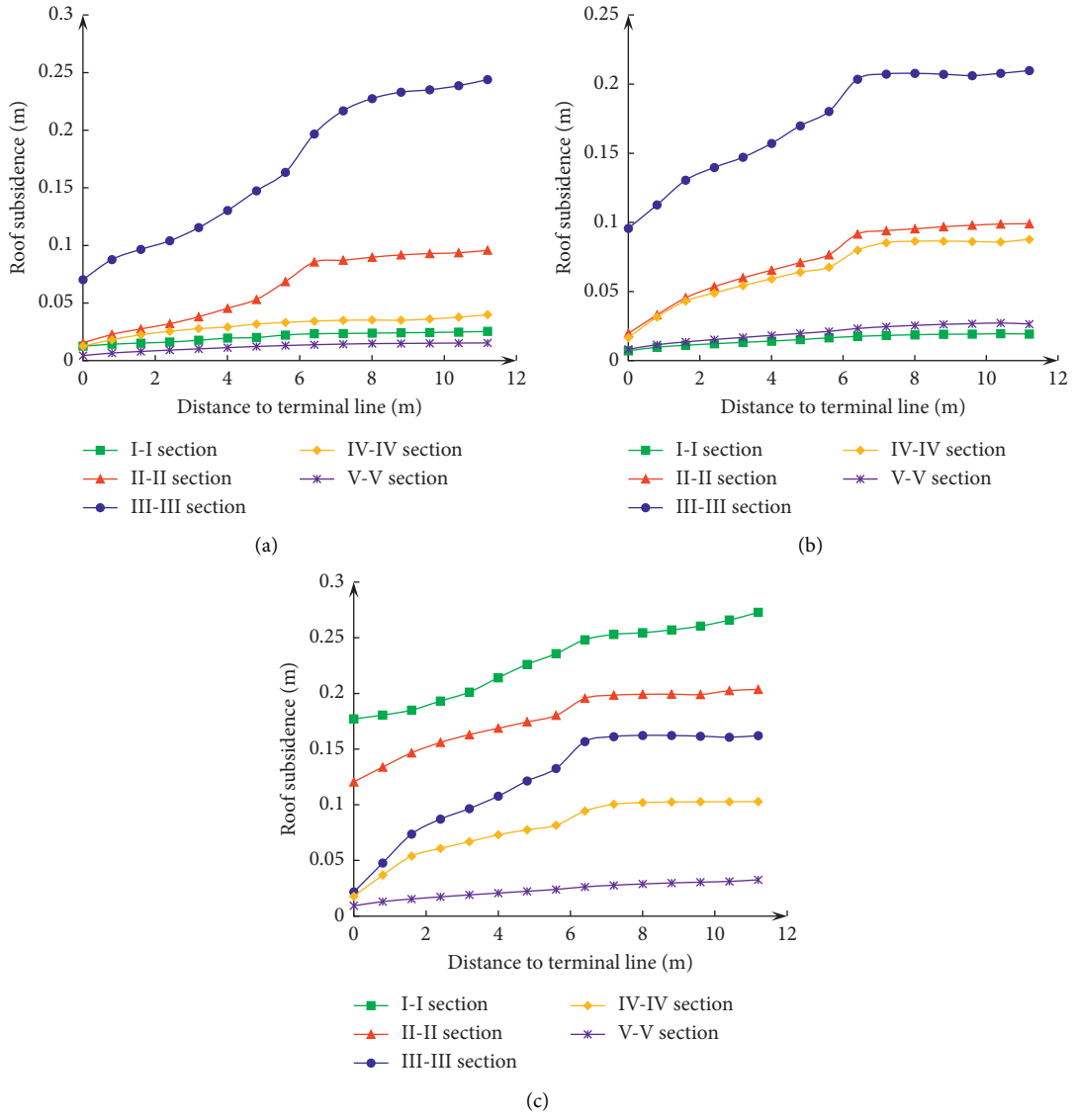

Figure 21: Roof subsidence curves of Stage II. (a) Scheme 1. (b) Scheme 2. (c) Scheme 3.

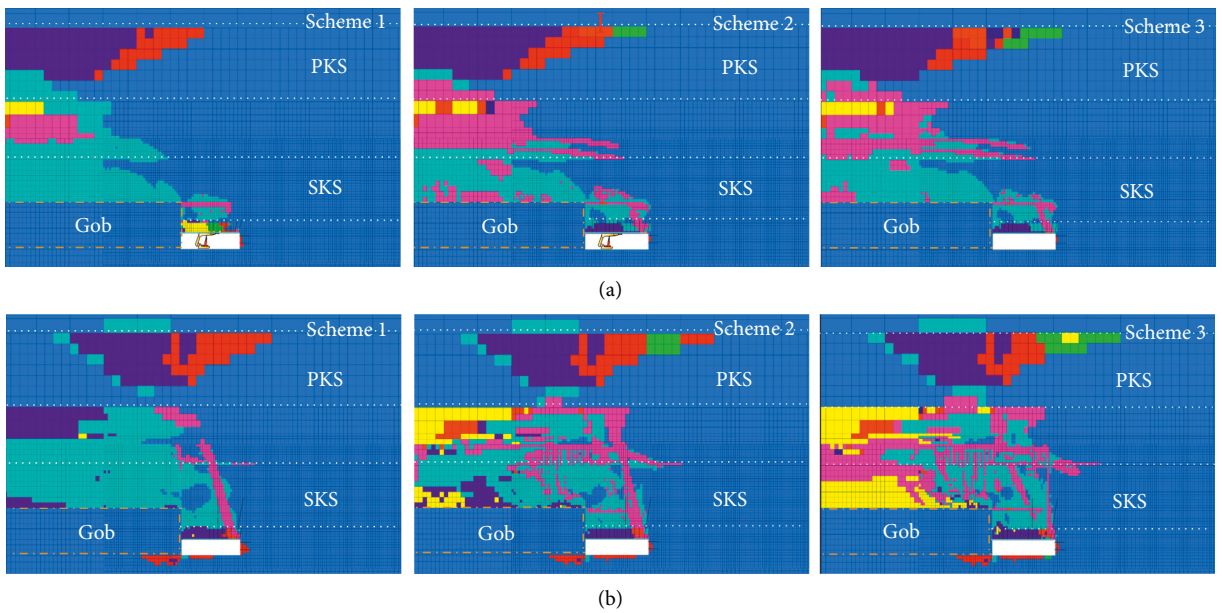

Figure 22: Continued.

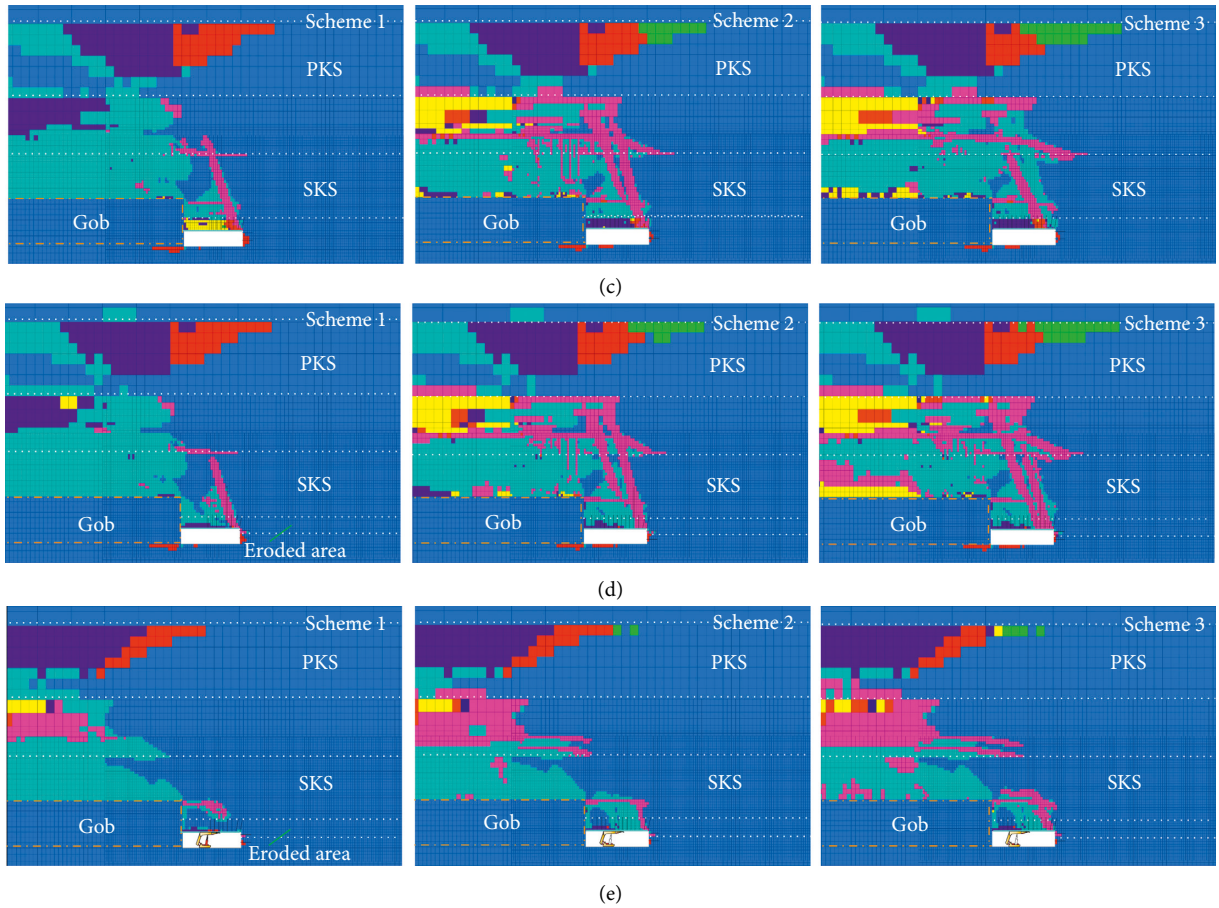

Figure 22: Plastic zone distribution of Stage III. (a) I-I. (b) II-II. (c) III-III. (d) IV-IV. (e) V-V.

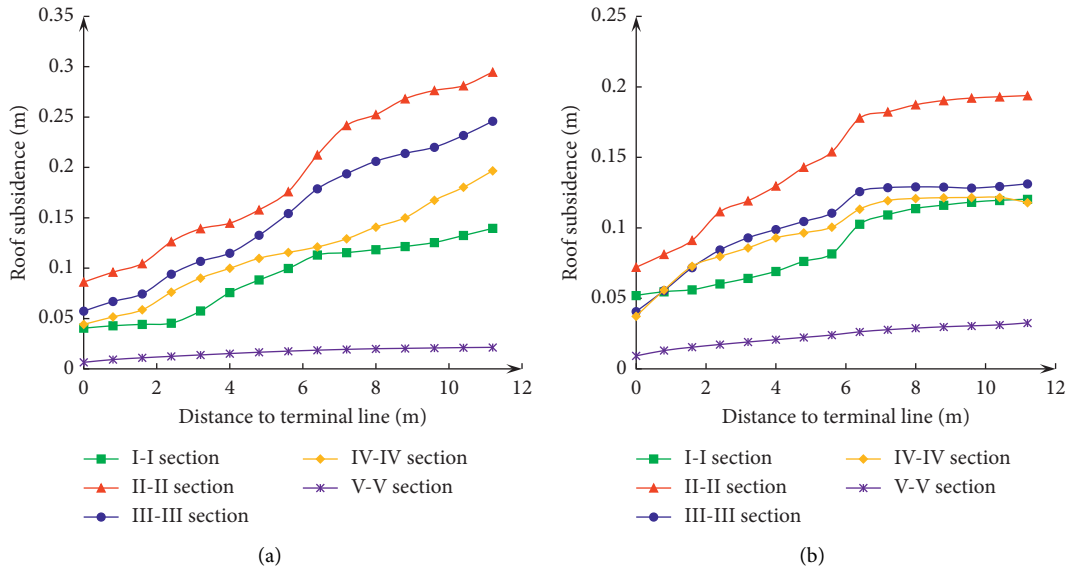

Figure 23: Continued.

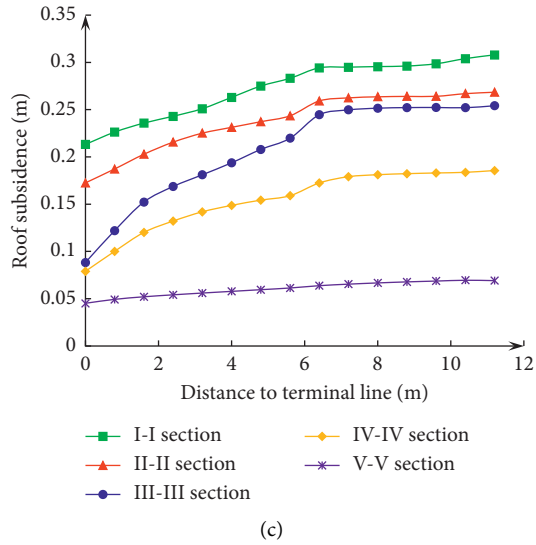

(c)

Figure 23: Roof subsidence curves of Stage III. (a) Scheme 1. (b) Scheme 2. (c) Scheme 3.

(a) (b)

Figure 24: Control effect of the rock surrounding the recovery roadway during the extraction of supports.

7. Conclusions

This paper mainly studied the stability control of the rock surrounding DKS recovery roadways in shallow seams. The principle and application conditions of pressure relief technology are introduced. The reasonable working resistances of the supports outside and inside the eroded area during pressure relief and equipment extraction were calculated. The support design of the recovery roadway and extraction scheme was improved. The main conclusions are as follows:

(i) Strong periodic weighting in the DKS is necessary before the extraction of equipment to release the accumulated rock pressure in the roof. The pressure relief technology should be reasonably applied based on the roof conditions and the periodic weighting law.

(ii) The yield load of the support inside the eroded area is somewhat low during pressure relief. Therefore, the strengthening support scheme of installing individual hydraulic props on both sides of hydraulic support is proposed.

(iii) The roof of the recovery roadway is supported by the CSHG structure. The reasonable working resistance of the support is no less than 5,294 kN during the extraction of equipment. The support design of the recovery roadway was improved based on the time effects of plastic zone development. The numerical simulation results showed that the development range of the plastic zone in the surrounding rock and the roof subsidence was reduced after the improved support design was applied.

(iv) The control effects of thee surrounding rock in three extraction schemes were simulated based on the constitutive model of the gob and the support. The results show that the surrounding rock control effect of Scheme 1, which combined the improved support design and the bidirectional extraction of equipment, is the best. Engineering application shows that Scheme 1 realizes the safe, economical, and rapid extraction of equipment.

Therefore, the key to stability control of the rock surrounding DKS recovery roadways in shallow seams is ensuring that the support has a reasonable working resistance,

enhancing the supporting efficiency of the roadway, and speeding up the extraction of equipment.

Data Availability

Some data used to support the findings of this study are included within the article. Other data used to support the findings of this study are available from the corresponding author upon request.

Conflicts of Interest

The authors declare that there are no conflicts of interest related to the publication of this manuscript.

Acknowledgments

This work was financially supported by the National key R&D program of China (No. 2018YFC0604701), the Natural Science Foundation of Jiangsu Province (No. BK20181358), the Postgraduate Research & Practice Innovation Program of Jiangsu Province (No. KYCX19_2131), the Postgraduate Research & Practice Innovation Program of China University of Mining and Technology (No. KYCX19_2131), and the Priority Academic Program Development of Jiangsu Higher Education Institutions.

References

[1] Q. X. Huang, "Ground pressure behavior and definition of shallow seams," *China Journal of Rock Mechanics and Engineering*, vol. 21, no. 8, pp. 1174–1177, 2002.

[2] R. Singh, P. K. Mandal, A. K. Singh, R. Kumar, J. Maiti, and A. K. Ghosh, "Upshot of strata movement during underground mining of a thick coal seam below hilly terrain," *International Journal of Rock Mechanics and Mining Sciences*, vol. 45, no. 1, pp. 29–46, 2008.

[3] J. Ju, J. Xu, and W. Zhu, "Longwall chock sudden closure incident below coal pillar of adjacent upper mined coal seam under shallow cover in the Shendong coalfield," *International Journal of Rock Mechanics and Mining Sciences*, vol. 77, pp. 192–201, 2015.

[4] W. Zhu, J. Xu, and Y. Li, "Mechanism of the dynamic pressure caused by the instability of upper chamber coal pillars in Shendong coalfield, China," *Geosciences Journal*, vol. 21, no. 5, pp. 729–741, 2017.

[5] C. Wang, C. Zhang, X. Zhao, L. Liao, and S. Zhang, "Dynamic structural evolution of overlying strata during shallow coal seam longwall mining," *International Journal of Rock Mechanics and Mining Sciences*, vol. 103, pp. 20–32, 2018.

[6] D. F. Zhu, S. H. Tu, H. S. Tu, and Z. Q. Yang, "Mechanisms of support failure and prevention measures under double-layer room mining gobs—a case study: Shigetai coal mine," *International Journal of Mining Science and Technology*, 2018.

[7] F. Wang, C. Duan, S. Tu, N. Liang, and Q. Bai, "Hydraulic support crushed mechanism for the shallow seam mining face under the roadway pillars of room mining goaf," *International Journal of Mining Science and Technology*, vol. 27, no. 5, pp. 853–860, 2017.

[8] D. Zhu and S. Tu, "Mechanisms of support failure induced by repeated mining under gobs created by two-seam room mining and prevention measures," *Engineering Failure Analysis*, vol. 82, pp. 161–178, 2017.

[9] Q. X. Huang, J. L. Zhou, L. T. Ma, and P. F. Tang, "Double key strata structure analysis of large mining height longwall face in nearly shallow coal seam," *Journal of China Coal Society*, vol. 42, no. 10, pp. 2504–2510, 2017.

[10] J. Ju and J. Xu, "Surface stepped subsidence related to top-coal caving longwall mining of extremely thick coal seam under shallow cover," *International Journal of Rock Mechanics and Mining Sciences*, vol. 78, pp. 27–35, 2015.

[11] X. Liu, G. Song, and X. Li, "Classification of roof strata and calculation of powered support loads in shallow coal seams of China," *Journal of the Southern African Institute of Mining and Metallurgy*, vol. 115, no. 11, pp. 1113–1119, 2015.

[12] Z. Meng, X. Shi, and G. Li, "Deformation, failure and permeability of coal-bearing strata during longwall mining," *Engineering Geology*, vol. 208, pp. 69–80, 2016.

[13] H. Wang, D. Zhang, X. Wang, and W. Zhang, "Visual exploration of the spatiotemporal evolution law of overburden failure and mining-induced fractures: a case study of the Wangjialing coal mine in China," *Minerals*, vol. 7, no. 3, p. 35, 2017.

[14] Z. G. Liu, Z. L. Fan, and Y. J. Zhang, "Fracture characteristics of overlying bedrock and clay aquiclude subjected to shallow coal seam mining," *Mine Water and the Environment*, vol. 38, no. 1, pp. 136–147, 2018.

[15] W. Yan, H. Dai, and J. Chen, "Surface crack and sand inrush disaster induced by high-strength mining: example from the Shendong coal field, China," *Geosciences Journal*, vol. 22, no. 2, pp. 347–357, 2018.

[16] A. Majdi, F. P. Hassani, and M. Y. Nasiri, "Prediction of the height of destressed zone above the mined panel roof in longwall coal mining," *International Journal of Coal Geology*, vol. 98, pp. 62–72, 2012.

[17] Z. Hu, C. Chen, W. Xiao, X. Wang, and M. Gao, "Surface movement and deformation characteristics due to high-intensive coal mining in the windy and sandy region," *International Journal of Coal Science & Technology*, vol. 3, no. 3, pp. 339–348, 2016.

[18] Y. Xu, K. Wu, L. Li, D. Zhou, and Z. Hu, "Ground cracks development and characteristics of strata movement under fast excavation: a case study at Bulianta coal mine, China," *Bulletin of Engineering Geology and the Environment*, vol. 78, no. 1, pp. 325–340, 2017.

[19] L. Yu, Z. Z. Fan, and G. Xu, "Study on the structure characteristics and ground pressure behavior of overlying strata with shallow buried coal seam," *Advanced Materials Research*, vol. 255-260, pp. 3780–3785, 2011.

[20] F. Wang, S. Tu, Y. Yuan, Y. Feng, F. Chen, and H. Tu, "Deep-hole pre-split blasting mechanism and its application for controlled roof caving in shallow depth seams," *International Journal of Rock Mechanics and Mining Sciences*, vol. 64, pp. 112–121, 2013.

[21] J. Ning, J. Wang, L. Jiang, N. Jiang, X. Liu, and J. Jiang, "Fracture analysis of double-layer hard and thick roof and the controlling effect on strata behavior: a case study," *Engineering Failure Analysis*, vol. 81, pp. 117–134, 2017.

[22] C. Liu, H. M. Li, D. J. Jiang, H. G. Li, and J. F. Feng, "Effects of immediate roof thickness on lower inferior key stratum movement in ends of large mining height panel," in *Proceedings of the 3rd International Symposium on Mine Safety Science and Engineering*, pp. 625–633, ISMS, Montreal, Canada, August 2016.

[23] W.-B. Guo, H.-S. Wang, G.-W. Dong, L. Li, and Y.-G. Huang, "A case study of effective support working resistance and roof support technology in thick seam fully-mechanized face

mining with hard roof conditions," *Sustainability*, vol. 9, no. 6, p. 935, 2018.

[24] X. F. Wang, D. S. Zhang, M. T. Xu, G. W. Fan, Z. H. Yang, and D. D. Qin, "Roof instability mechanism of longwall coalface for sandy soil gullies overlaying shallow seams," *Disaster Adv.*, vol. 6, pp. 260–267, 2013.

[25] Z. Li, J. Xu, J. Ju, W. Zhu, and J. Xu, "The effects of the rotational speed of voussoir beam structures formed by key strata on the ground pressure of stopes," *International Journal of Rock Mechanics and Mining Sciences*, vol. 108, pp. 67–79, 2018.

[26] C. He and J. Xu, "Subsidence prediction of overburden strata and surface based on the voussoir beam structure theory," *Advances in Civil Engineering*, vol. 2018, Article ID 2606108, 13 pages, 2018.

[27] J. Wang, S. Yang, Y. Li, and Z. Wang, "A dynamic method to determine the supports capacity in longwall coal mining," *International Journal of Mining, Reclamation and Environment*, vol. 29, no. 4, pp. 277–288, 2015.

[28] J. Guo, G. Feng, P. Wang, T. Qi, X. Zhang, and Y. Yan, "Roof strata behavior and support resistance determination for ultra-thick longwall top coal caving panel: a case study of the Tashan coal mine," *Energies*, vol. 11, no. 5, p. 1041, 2018.

[29] G. S. P. Singh and U. K. Singh, "Numerical modeling study of the effect of some critical parameters on caving behavior of strata and support performance in a longwall Working," *Rock Mechanics and Rock Engineering*, vol. 43, no. 4, pp. 475–489, 2010.

[30] C. Zhang, S. Tu, L. Zhang, Q. Bai, Y. Yuan, and F. Wang, "A methodology for determining the evolution law of gob permeability and its distributions in longwall coal mines," *Journal of Geophysics and Engineering*, vol. 13, no. 2, pp. 181–193, 2016.

[31] Q. Bai, S. Tu, F. Wang, and C. Zhang, "Field and numerical investigations of gateroad system failure induced by hard roofs in a longwall top coal caving face," *International Journal of Coal Geology*, vol. 173, pp. 176–199, 2017.